Ceramics International 46 (2020) 16068–16073

Contents lists available at ScienceDirect

Ceramics International

journal homepage: www.elsevier.com/locate/ceramint

Fabrication of ultra-high-temperature nonstoichiometric hafnium carbonitride via combustion synthesis and spark plasma sintering

V.S. Buinevich[a], A.A. Nepapushev[a], D.O. Moskovskikh[a,*], G.V. Trusov[a], K.V. Kuskov[a], S.G. Vadchenko[b], A.S. Rogachev[b], A.S. Mukasyan[c]

[a] National University of Science and Technology MISIS, Moscow, 119049, Russia
[b] Institute of Structural Macrokinetics and Material Science, Russian Academy of Sciences, Chernogolovka, Moscow, 142432, Russia
[c] Department of Chemical and Biomolecular Engineering, University of Notre Dame, Notre Dame, IN, 46556, USA

ARTICLE INFO

Keywords:
Ultra-high-temperature ceramics
Hafnium carbonitride
High-energy ball milling
Combustion synthesis
Spark plasma sintering

ABSTRACT

In this study, nonstoichiometric hafnium carbonitrides (HfC_xN_y) were fabricated via short-term (5 min) high-energy ball milling of Hf and C powders, followed by combustion of mechanically induced Hf/C composite particles in a nitrogen atmosphere (0.8 MPa). The obtained $HfC_{0.5}N_{0.35}$ powder exhibited a rock-salt crystal structure with a lattice parameter of 0.4606 nm. The melting point of this synthesized ceramic material was experimentally shown to be higher than that of binary hafnium carbide (HfC). The nonstoichiometric hafnium carbonitride was then consolidated under a constant pressure of 50 MPa at a temperature of 2000 °C and a dwelling time of 10 min, through spark plasma sintering. The obtained bulk ceramic material had a theoretical material density of 98%, Vickers hardness of 21.3 GPa, and fracture toughness of 4.7 MPa $m^{1/2}$.

1. Introduction

Carbides and nitrides of transition metals (groups IVB and VB) possess a unique set of properties, including high density, chemical durability, corrosion resistance, and exceptionally high melting point [1–4], which makes them attractive for a variety of applications, specifically under extreme temperatures [5]. For example, ultra-high-temperature ceramics (UHTC) based on these phases can be used as a thermal protection system in supersonic jets and as parts of combustion chambers or rocket nozzles [6–11]. For essentially stoichiometric hafnium carbide ($HfC_{0,98}$), a melting point above 3927 °C was reported, which is the highest value measured for binary phases [12,13].

The ternary phases of these metals may have better mechanical properties [14–16] and even higher melting points [11,17]. For example, it was experimentally shown that Ta_4HfC_5 ceramics might have a melting point as high as 4027 ± 80 °C [18]. According to theoretical calculations, hafnium carbonitride with nonstoichiometric $HfC_{0.51}N0_{0.38}$ phase composition should have a melting point above 4200 °C [17]. Other theoretical work [11] predicts that a melting point of ~4057 °C corresponds to a 0.76HfC–0.24HfN phase composition. It is worth noting that both calculation methods, i.e., ab initio molecular dynamics calculation [17] and the machine learning approach [11], suggest that the Hf–C–N system should hold a record high melting temperature. Moreover, the addition of any other refractory components, e.g., tantalum, does not lead to an increase in this value.

Hafnium carbonitride was obtained as a thin layer by chemical vapor deposition [19] and magnetron sputtering [20,21] methods. High-energy ball milling (HEBM) of a hafnium and carbon mixture in a nitrogen atmosphere was used to produce stoichiometric HfC_xN_{1-x} powders by mechanically induced self-sustained reactions [22,23]. An energy-efficient combustion synthesis (CS) approach based on thermally initiated self-sustained exothermic reactions [24–26] was also utilized to produce different stoichiometric MeC_xN (Me = Ti, V, or Hf) carbonitrides powders [27–33]. Essentially, no data are available on the combustion synthesis of hafnium carbonitrides or on the fabrication of bulk hafnium carbonitride ceramics.

In this study, we developed and applied a novel synergetic strategy to produce bulk-ceramic-based nonstoichiometric (HfC_xN_y, where $x + y < 1$) hafnium carbonitride. This approach includes three steps: (i) short-term HEBM of hafnium and carbon in an inert atmosphere to fabricate reactive Hf/C nanostructured composites, (ii) combustion of these particles in a nitrogen atmosphere in the CS regime to produce HfC_xN_y powder, and (iii) spark plasma sintering (SPS) [34–36] of nonstoichiometric hafnium carbonitrides powder to fabricate bulk UHTC. The properties of these produced UHTC are investigated and discussed.

* Corresponding author.
E-mail address: mos@misis.ru (D.O. Moskovskikh).

https://doi.org/10.1016/j.ceramint.2020.03.158
Received 31 December 2019; Received in revised form 12 March 2020; Accepted 14 March 2020
Available online 17 March 2020

2. Methods and Materials

Powders of hafnium (GFM-1, SMM, Russia; purity = 98.7%), carbon (P804T, Russia; purity = 99.5%), and nitrogen (LLC "GAZEXPO," Russia; purity = 99.99%) were used as precursors. The Hf and C powders in a 2:1 mol ratio were ball milled for 5 min in a steel jar in a planetary mill "Activator 2S" (Aktivator, Novosibirsk, Russia) with a steel ball to a powder ratio of 20:1. The milling speed was 694 rpm and the rotational coefficient was $K = 1$. This prepared reactive Hf/C loose powder was placed inside a laboratory chemical reactor. The reactor was vacuumed and then filled with pure gaseous nitrogen up to a pressure of 0.8 MPa. The powder was locally preheated by a hot tungsten wire to initiate chemical reactions and a self-sustained combustion front self-propagated through the medium, leading to the formation of the hafnium carbonitride powder. This synthesized powder was consolidated under a nitrogen atmosphere using an SPS device (Labox 650, SinterLand, Japan). A load of 50 MPa was continuously applied to the sample during the process. The heating rate was 100 °C/min. Consolidation was conducted at 2000 °C with a dwelling time of 10 min. Through this process, we fabricated bulk ceramic disks with a diameter of 15 mm and a thickness of 2–3 mm.

The phase composition of the fabricated materials was studied through an X-ray diffraction (XRD) analysis on a DRON-4-07 (Russia) using monochromatic Co-Kα radiation (λ = 0.1788 nm). XRD patterns were scanned from 30° to 110° (2Θ) in a step-by-step scanning mode with a scan increment of 0.1°. The exposure time was 2 s. The International Centre for Diffraction Data Powder Diffraction File (PDF) bases were used for processing the XRD patterns. The interplanar distances (d_{hkl}, in nanometers) between reflective planes with (hkl) Miller indices were calculated using Bragg's equation:

$$n\lambda = 2d_{hkl}sin\theta, \quad (1)$$

where n is an integer describing the order of the diffraction reflection, λ is the wavelength (Co) of the incident beam (in nanometers), and θ is the angle of incidence.

The microstructure of the ceramics was analyzed using a scanning electron microscope (SEM; Jeol JSM7600F, Japan) equipped with an energy dispersive X-Ray spectroscopy (EDS) microanalysis system (INCA SDD 61 X-MAX, Oxford Instruments). SEM imaging and EDS analyses were performed at an acceleration voltage of 15 keV. The relative density of the sintered samples was determined using the ImageJ software package for image analysis. The method is based on the use of a graphical tool, which divides all the colors that are on opposite sides of a given brightness threshold into black and white. Based on the scale of the sample's SEM image, it is possible to calculate the total area of the pores in the sample [37].

The materials' density (ρ) was determined using the Archimedes method on an analytic scale (Sartorius ME235), with no fewer than ten measurements in air and distilled water (ρ_w = 0.9978 g/cm^3). Vaseline (ρ_p = 0.870 g/cm^3) acted as a protective layer. The density was calculated from

$$\rho = \frac{m_1\rho_w\rho_p}{(m_2 - m_3)\rho_p - m_4\rho_w}, \quad (2)$$

where m_1 is the sample mass without a protective layer in air (in grams); m_2 is the mass of the sample with a protective layer in air (in grams); m_3 is the mass of the sample with a protective layer in water (in grams); and m_4 is a mass of the protective layer (in grams).

The Vickers hardness (HV, in gigapascals) and the fracture toughness (K_{1c}, in MPa·m$^{1/2}$) were determined using a Struers DuraScan 70 digital device. At least ten hardness measurements were taken for each sample. The tests were conducted using a Vickers diamond tip, under a maximum load of 9.8 kg and a strain exposure time of 20 s. The hardness was calculated according to

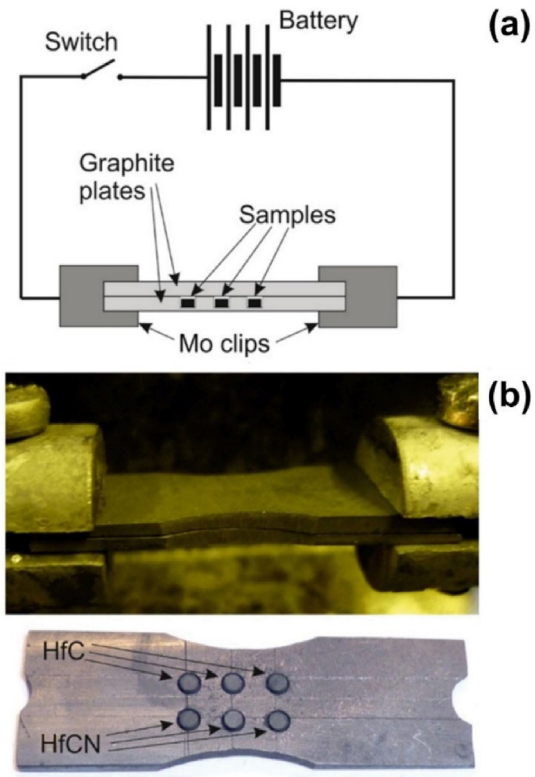

Fig. 1. (a) Schematic and (b) photograph of the setup used for the comparative studies of the ceramics' melting point.

$$HV = 1{,}854\frac{P}{d^2}, \quad (3)$$

where P is the applied load (in kilograms) and d is the length of the indented diagonal (in millimeters).

The fracture toughness was calculated by using the Anstis formula:

$$K_{1c} = 0.016\left(\frac{E}{HV}\right)^{\frac{1}{2}} \times \frac{P}{c^{\frac{3}{2}}}, \quad (4)$$

where P (in newtons) is the load, c (in meters) is the crack length from the center of the indent to the crack tip in meters, and E (in gigapascals) is Young's modulus. Modulus values were taken from Ref. [38].

Although we could not directly measure the melting point of the fabricated ceramics, we compared the obtained hafnium carbonitride with commercial hafnium carbide (HfC). The experimental setup is presented in Fig. 1. Disk-like specimens (3 mm in diameter and 1–2 mm in height), compacted from commercial HfC and synthesized HfC_xN_y, were placed in the niches along the graphite strip, which had a dumbbell shape narrowing in the middle. The samples were arranged in two parallel lines alongside the plates, and each line consisted of three identical samples (Fig. 1a). The strip was covered with a graphite plate of similar geometry to avoid heat loss through radiation from the samples. This graphite "sandwich" was installed between two Mo electrodes. A powerful battery (with a current and voltage of up to 1200 A and 14 V, respectively) was used for Joule heating of the entire configuration. The tests were conducted in a vacuum chamber under a high vacuum of 10^{-4} Pa. Because of the varying width of the strip, the highest temperature was achieved in its narrowest part, i.e., in the middle of the heater. The temperature gradually decreased toward the wider ends of the graphite plates attached to the Mo clips. The melting points of the specimens were determined by comparing their microstructures before and after the heating.

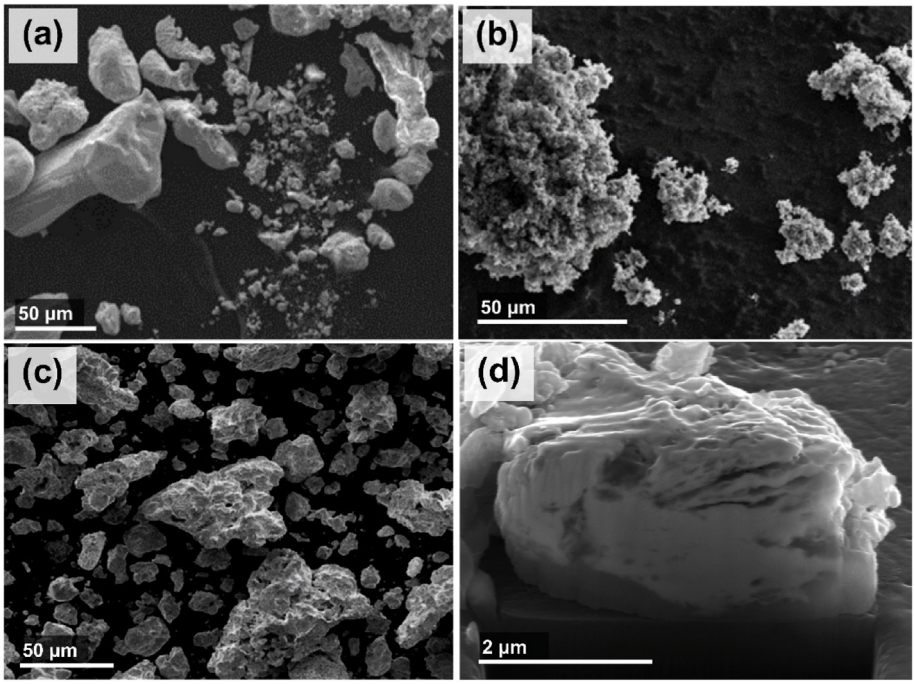

Fig. 2. SEM images of (a) initial hafnium powder, (b) carbon black, (c) composite Hf/C particles, and (d) cross section of the composite Hf/C particles.

3. Results and discussion

SEM studies of the precursor show that hafnium powder has a wide range (10–100 μm) of particle size (Fig. 2a). The amorphous carbon black consists of agglomerates of nanoparticles with an average size of ~100 nm (Fig. 2b). Short-term (5 min) HEBM of a Hf + 0.5C mixture in an inert (argon) dry atmosphere leads to the formation of composite Hf/C particles with sizes in the range of 20–100 μm (Fig. 2c). Analysis of cross sections of such particles reveals that they comprise hafnium (light) and carbon (dark) phases (Fig. 2d). An XRD analysis of as-milled powder (Fig. 3a) reveals that the powder indeed predominately consists of pure crystalline hafnium, and only traces of the hafnium carbide phase can be detected. Therefore, 5 min of HEBM is determined to be the critical milling time that does not lead to the formation of the product, which diminishes the reactivity of the system.

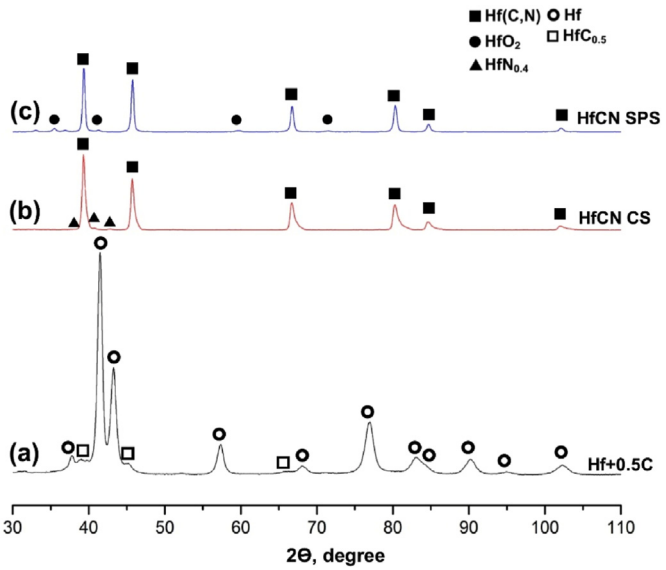

Fig. 3. XRD patterns for the (a) as-milled Hf/C particles, (b) Hf(C,N) powder after combustion synthesis, and (c) Hf(C,N) ceramic after SPS.

Notably, under the investigated conditions, i.e., a nitrogen pressure of 0.8 MPa, the self-sustained combustion reaction cannot proceed in the Hf + 0.5C mixture obtained via conventional mixing. However, after short-term HEBM, the CS process can be easily initiated. The XRD analysis of the combustion product is presented in Fig. 3b. It can be seen that the product primarily consists of hafnium carbonitride, with only traces of a hafnium nitride phase. Moreover, during the rapid CS process, the nitrogen content in different HfC_xN_y particles varied slightly (see the Supplementary file). This variation led to the asymmetry of the XRD peaks. The *d* spacings for the HfN and HfC standards and the obtained Hf(C, N) phases are summarized in Table 1. The calculated lattice constant for the obtained (NaCl) Fm-3m (225) crystal structure is 0.4606 nm.

The microstructure of the Hf(C,N) powder is shown in Fig. 4. It can be seen by its morphology that the structure of synthesized ceramic mimics that of the composite Hf/C particles (compare Figs. 2c and 4a). Analysis of the powder's cross section suggests that it has a uniform structure with some pores and cavities inside (Fig. 4b). A closer look at the carbonitride structure indicates that it consists of small submicron grains (Fig. 4c). The EDS analysis indicates that the C to N ratio in the phase equals 1.42, and no free carbon was detected. Because the Hf to C ratio in the powder mixture was 1:0.5, one may estimate that the phase composition of the synthesized carbon nitride is $HfC_{0.5}N_{0.35}$.

The melting points of the commercial HfC and the Hf(C,N) fabricated using the HEBM + CS approach were compared using the method described above (Fig. 1). The macro image of a graphite heater with six specimens (three HfC samples in the upper row and three Hf(C,N)

Table 1
d spacing for the HfC and HfN standards and Hf(C,N) after CS and SPS.

Material	(NaCl) Fm-3m (225)					
	(111)	(200)	(220)	(311)	(222)	(400)
HfC (PDF #65–7113)	2.6737	2.3155	1.6373	1.3963	1.3369	1.1578
HfN (PDF #65–4298)	2.6073	2.2580	1.5967	1.3616	1.3037	1.1290
Hf(C,N) CS	2.6593	2.3048	1.6275	1.3869	1.3292	1.1503
Hf(C,N) SPS	2.6570	2.2995	1.6270	1.3875	1.3275	1.1501

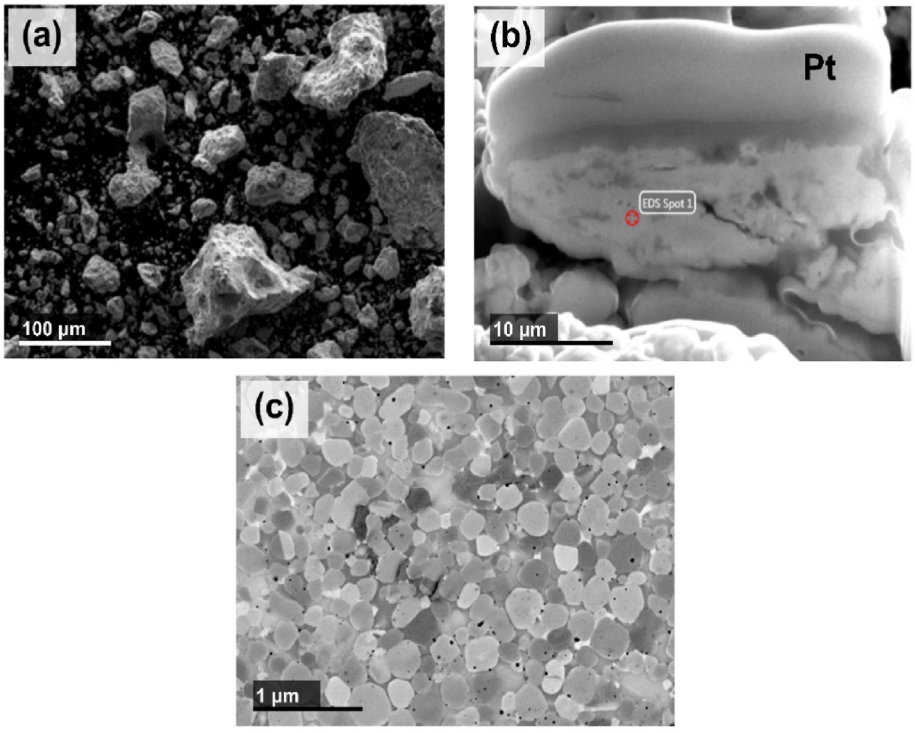

Fig. 4. Microstructure of the synthesized Hf(C,N) particles: (a) general view; (b,c) cross sections.

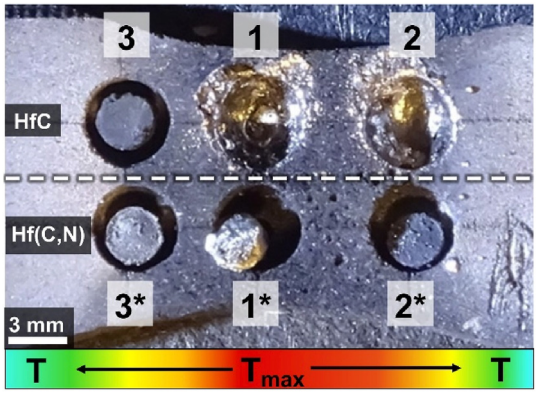

Fig. 5. Macro image of the graphite heater with the samples after comparative experiments on the melting points of ceramics.

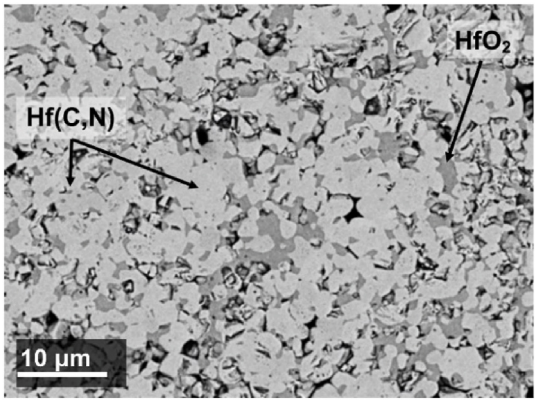

Fig. 7. Typical microstructure of consolidated Hf(C,N) ceramic.

samples in the lower row) after one of the experiments is shown in Fig. 5. As mentioned earlier, the highest temperature was observed in the middle of the heater (samples 1 and 1*), where the graphite plate has the narrower cross section (20.1 mm^2) and hence the highest electric current density. The temperature decreased toward the clamped edges of the plate and, based on the cross-sectional area (22.35 and 23.85 mm^2 for lines 2–2* and 3–3*, respectively), it can be

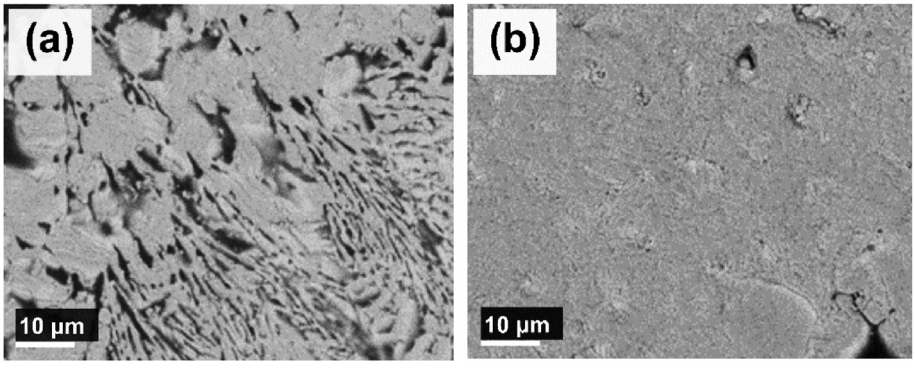

Fig. 6. Microstructures of the ceramics after heating: (a) HfC; (b) Hf(C,N).

Table 2
Mechanical properties of Hf-based ceramics.

Material	Hardness HV_{10}, (GPa)	Fracture toughness K_{1c} (MPa $m^{1/2}$)	Relative density (%)
Hf(C,N) [this work]	21.3 ± 0.55	4.7 ± 0.30	98.1 ± 0.2
HfC [39]	18.8 ± 0.70	not available	98
HfC [40]	23.14 ± 0.45	3.00 ± 0.18	100

concluded that temperature for samples 2 and 2* should be higher than that for samples 3 and 3*. Therefore, the following temperature relation can be established during the experiment: $T_3 < T_2 < T_1$. Fig. 5 shows that, under the investigated conditions, neither sample at temperature T_3 melted and they completely retained their shape. At T_2, the samples behaved differently; i.e., HfC (sample 2) partially melted and changed its shape; however, Hf(C,N) (sample 2*) maintained its shape. Finally, in the hottest zone (T_1), HfC (sample 1) completely melted and filled the cylindrical hole and even spread along the graphite surface, while HfC_xN_y (sample 1*) only shrunk as a result of sintering.

The microstructures of samples 1 and 1* after heat treatment are shown in Fig. 6. The dendritic structure, formed during solidification of the HfC melt (Fig. 6a), and the unaltered microstructure of bulk Hf(C,N) confirmed the aforementioned conclusion regarding the structural transformation that occurred during heating. Note that qualitatively similar behavior was observed in all three experiments. The melting point of synthesized hafnium carbonitride must therefore necessarily be higher than that of HfC, which is considered to be one of the most refractory compounds. Precise measurement of the melting points for the synthesized ceramics will constitute the topic for a follow-up study.

The nonstoichiometric Hf(C, N) powder was consolidated via SPS under the conditions described in the Methods and Materials section. The dwelling time at a maximum temperature of 2000 °C was 10 min. The density of the obtained ceramic material was 11.89 ± 0.05 g/cm^3, which corresponds to 98.1 ± 0.2 of the theoretical material density according to the microstructure analysis. The XRD analysis of the compacted ceramic is shown in Fig. 3c. It can be seen that the crystal structure of the bulk material is essentially identical to that of the Hf(C,N) powder used. The calculated lattice constant is 0.4602 nm (compared with 0.4606 nm for the initial powder). Some amount of a HfO_2 phase was also detected. The microstructure of the compacted ceramic is shown in Fig. 7. The grain size of the Hf(C,N) phase (light in color) is on the order of 5 μm. Some areas (gray) of the HfO_2 phase are can be observed. Based on the chemical analysis of total oxygen in the CS powder (0.57 wt%) and sintered material (~ 1 wt%), we made a rough estimation of the HfO_2 phase content. Assuming that all detected oxygen was in the HfO_2 phase, we estimated ~ 4 wt% and ~ 9 wt% for the HfO_2 phase in the CS powder and SPS material, respectively. There are two reasons for the appearance of an oxide phase. The first is related to the oxygen content in the initial hafnium powder (~ 0.5 wt%). The second is the oxidation of carbonitride [40] in the sintering atmosphere.

The mechanical properties of the ceramics and HfC bulk materials in other studies are summarized in Table 2. It can be seen that, with comparable densities, the hardness and fracture toughness of Hf(C,N) ceramics is higher than that for HfC material sintered at 2200 °C for 10 min [39]. The fully dense HfC ceramic obtained after 10 min of consolidation at 1900 °C exhibits slightly higher hardness but lower fracture toughness [40].

4. Conclusion

It was theoretically predicted [11,17] that nonstoichiometric hafnium carbonitrides should exhibit extremely high melting points exceeding 4000 °C. Hafnium carbonitrides produced by other approaches, e.g., reactive HEBM [22,23], are characterized by stoichiometric compositions, i.e., HfC_xN_{1-x}. The combination of short-term (5 min) HEBM and combustion synthesis allowed us to fabricate nonstoichiometric $HfC_{0.5}N_{0.35}$ carbonitride. The explanation for achieving this type of compound is as follows: HEBM led to the formation of composite Hf/C highly reactive particles with the desired, i.e., 1:0.5, ratio between metal and nonmetal. Recall that, without HEBM, it is virtually impossible to initiate a self-sustaining reaction in the Hf–C system. The Hf/C particles were subjected to the combustion reaction under a nitrogen atmosphere. It is worth noting that both reactions, i.e., between Hf and carbon, as well as between Hf and nitrogen, are highly exothermic [41]. The amount of carbon in the crystal structure of the combustion product was determined by the composition of the Hf/C particles (1:0.5). At the same time, optimized nitrogen pressure (0.8 MPa) enabled additional self-nitridation to the desired nitrogen content. All the aforementioned points suggest that a combination of short-term HEBM and combustion synthesis is a unique tool for producing nonstoichiometric multicomponent phases.

It is difficult to measure a material's melting points when it exceeds 4000 °C. Therefore, we decided to compare the melting point values of the produced ceramics to that of extremely refractory HfC carbide, which probably exhibits a record high melting point temperature. Statistical analyses of the numerous experimental data on simultaneous heating of these materials revealed that the synthesized $HfC_{0.5}N_{0.35}$ carbonitride had a higher melting point than HfC did.

It was also demonstrated that SPS of the carbonitride under a constant pressure of 50 MPa at a temperature of 2000 °C and a dwelling time of 10 min allowed us to fabricate bulk ceramics with a relative density of ~98%. The measured mechanical properties, i.e., Vickers hardness HV = 21.3 GPa and fracture toughness K_{1c} = 4.7 MPa $m^{1/2}$, appeared to be comparable to or higher than those for HfC-based UHTC fabricated by SPS [39,40].

Acknowledgment

This study was conducted with financial support from the Russian Science Foundation (Grant No. 19-79-10280). Use of the setup for the comparative studies of the ceramics' melting point was made possible by support from the Ministry of Science and Higher Education of the Russian Federation in the framework of Increase Competitiveness Program of NUST«MISiS» (No. K2A-2018-056), implemented by a governmental decree dated 16 March 2013, N 211.

Appendix A. Supplementary data

Supplementary data to this article can be found online at https://doi.org/10.1016/j.ceramint.2020.03.158.

References

[1] H.O. Pierson, Handbook of refractory carbides and nitrides : properties, characteristics, processing, and applications, Handb. Refract. Carbides Nitrides. (1996) 362 ISBN: 9780815513926.
[2] X.-X. Yu, C.R. Weinberger, G.B. Thompson, Ab initio investigations of the phase stability in tantalum carbides, Acta Mater. 80 (2014) 341–349.
[3] A. Srivastava, B.D. Diwan, Structural and elastic properties of ZrN and HfN: ab initio study, Can. J. Phys. 92 (2014) 1058–1061.
[4] M. Chauhan, D.C. Gupta, Structural, electronic, mechanical and thermo-physical properties of TMN (TM = Ti, Zr and Hf) under high pressures: a first-principle study, Int. J. Refract. Metals Hard Mater. 42 (2014) 77–90.
[5] J. Binner, M. Porter, B. Baker, J. Zou, V. Venkatachalam, V.R. Diaz, et al., Selection, processing, properties and applications of ultra-high temperature ceramic matrix

composites, UHTCMCs – a review, Int. Mater. Rev. (2019) 1–56.
[6] T.H. Squire, J. Marschall, Material property requirements for analysis and design of UHTC components in hypersonic applications, J. Eur. Ceram. Soc. 30 (2010) 2239–2251.
[7] E. Wuchina, E. Opila, M. Opeka, W. Fahrenholtz, I. Talmy, UHTCs: ultra-High Temperature Ceramic materials for extreme environment applications, Electrochem. Soc. Interface, 2007, pp. 30–36.
[8] W.G. Fahrenholtz, E.J. Wuchina, W.E. Lee, Y. Zhou, Ultra-High Temperature Ceramics, John Wiley & Sons, Inc, Hoboken, NJ, NJ, 2014.
[9] A. Mukhopadhyay, G.B. Raju, B. Basu, Ultra high temperature ceramics, MAX Phases Ultra-high Temp. Ceram. Extrem. Environ, IGI Global, 2013, pp. 49–99.
[10] I.M. Low, Y. Sakka, C.F. Hu, MAX Phases and Ultra-high Temperature Ceramics for Extreme Environments, IGI Global, 2013.
[11] N. Qu, Y. Liu, M. Liao, Z. Lai, F. Zhou, P. Cui, et al., Ultra-high temperature ceramics melting temperature prediction via machine learning, Ceram. Int. 45 (2019) 18551–18555.
[12] M. Sheindlin, T. Falyakhov, S. Petukhov, G. Valyano, A. Vasin, Recent advances in the study of high-temperature behaviour of non-stoichiometric TaC x , HfC x and ZrC x carbides in the domain of their congruent melting point, Adv. Appl. Ceram. 117 (2018) s48–s55.
[13] O. Cedillos-Barraza, D. Manara, K. Boboridis, T. Watkins, S. Grasso, D.D. Jayaseelan, et al., Investigating the highest melting temperature materials: a laser melting study of the TaC-HfC system, Sci. Rep. 6 (2016) 37962.
[14] J. Kim, H. Lim, Y.J. Suh, H. Lim, S. Kang, Temperature-dependent stable phase domains of Zr–C–N (Zr–ZrC–ZrC0.96–Zr(C1 − xNx) − ZrN, x = 0.1–0.9) systems from ab initio calculations and experimental results, J. Alloys Compd. 692 (2017) 997–1003.
[15] V.V. Skripnyak, V.A. Skripnyak, Predicting the mechanical properties of ultra-high temperature ceramics, Lett. Mater. 7 (2017) 407–411.
[16] G. Hua, J. Zhong, Y. Qi, X. Cheng, Influence of carbon on stability, mechanical property, electronic structure, and lattice dynamics of silicon carbonitride, J. Am. Ceram. Soc. 101 (2018) 5717–5731.
[17] Q.-J. Hong, A. van de Walle, Prediction of the material with highest known melting point from ab initio molecular dynamics calculations, Phys. Rev. B 92 (2015) 020104.
[18] A.I. Savvatimskiy, S.V. Onufriev, S.A. Muboyadzhyan, Thermophysical properties of the most refractory carbide Ta0.8Hf0.2C under high temperatures (2000–5000 K), J. Eur. Ceram. Soc. 39 (2019) 907–914.
[19] W. Wang, T. Nabatame, N. Haneji, Y. Shimogaki, Electrical and thermal stability characteristics of HfCN films as metal gate-electrode synthesized by metalorganic chemical vapor deposition, Jpn. J. Appl. Phys. 44 (2005) L1019–L1021.
[20] W.F. Piedrahita, W. Aperador, J.C. Caicedo, P. Prieto, Evolution of physical properties in hafnium carbonitride thin films, J. Alloys Compd. 690 (2017) 485–496.
[21] W.F. Piedrahita, L.E. Coy, C. Amaya, I. Llarena, J.C. Caicedo, L. Yate, Influence of the negative R.F. bias voltage on the structural, mechanical and electrical properties of Hf–C–N coatings, Surf. Coating. Technol. 286 (2016) 251–255.
[22] E. Chicardi, C. García-Garrido, A.M. Beltrán, M.J. Sayagués, F.J. Gotor, Synthesis of a cubic Ti(BCN) advanced ceramic by a solid-gas mechanochemical reaction, Ceram. Int. 45 (2019) 3878–3885.
[23] J.M. Córdoba, M.J. Sayagués, M.D. Alcalá, F.J. Gotor, Monophasic nanostructured powders of niobium, tantalum, and hafnium carbonitrides synthesized by a mechanically induced self-propagating reaction, J. Am. Ceram. Soc. 90 (2007) 381–387.
[24] A.S. Mukasyan, D.O. Moskovskikh, A.A. Nepapushev, J.M. Pauls, S.I. Roslyakov, Ceramics from self-sustained reactions: recent advances, J. Eur. Ceram. Soc. (2019), https://doi.org/10.1016/j.jeurceramsoc.2019.12.028.
[25] G. Liu, K. Chen, J. Li, Combustion synthesis: an effective tool for preparing inorganic materials, Scripta Mater. 157 (2018) 167–173.
[26] A.S. Mukasyan, C.E. Shuck, J.M. Pauls, K.V. Manukyan, D.O. Moskovskikh, A.S. Rogachev, The solid flame phenomenon: a novel perspective, Adv. Eng. Mater. 20 (2018).
[27] I.P. Borovinskaya, Chemical classes of the SHS processes and materials, Pure Appl. Chem. 64 (1992) 919–940.
[28] M. Eslamloo-Grami, Z.A. Munir, The mechanism of combustion synthesis of titanium carbonitride, J. Mater. Res. 9 (1994) 431–435.
[29] C.L. Yeh, E.W. Liu, Preparation of tantalum carbonitride by self-propagating high-temperature synthesis of Ta-C system in nitrogen, Ceram. Int. 32 (2006) 653–658.
[30] C.L. Yeh, Y.D. Chen, Combustion synthesis of vanadium carbonitride from V-C powder compacts under nitrogen pressure, Ceram. Int. 33 (2007) 365–371.
[31] S. Dyjak, M. Wasilewska, S. Cudziło, Combustion synthesis of titanium carbonitrides, Cent. Eur. J. Energ. Mater. 12 (2015) 249–259.
[32] C.L. Yeh, Y.D. Chen, Direct formation of titanium carbonitrides by SHS in nitrogen, Ceram. Int. 31 (2005) 719–729.
[33] C.L. Yeh, Y.D. Chen, Synthesis of niobium carbonitride by self-propagating combustion of Nb–C system in nitrogen, Ceram. Int. 31 (2005) 1031–1039.
[34] E.A. Olevsky, D.V. Dudina, Field-Assisted Sintering, Springer International Publishing, Cham, 2018.
[35] M. Abedi, D.O. Moskovskikh, A.S. Rogachev, A.S. Mukasyan, Spark plasma sintering of titanium spherical particles, Metall. Mater. Trans. B 47 (2016) 2725–2731.
[36] R. Licheri, C. Musa, R. Orrù, G. Cao, D. Sciti, L. Silvestroni, Bulk monolithic zirconium and tantalum diborides by reactive and non-reactive spark plasma sintering, J. Alloys Compd. 663 (2016) 351–359.
[37] D.O. Moskovskikh, Y.-C. Lin, A.S. Rogachev, P.J. McGinn, A.S. Mukasyan, Spark plasma sintering of SiC powders produced by different combustion synthesis routes, J. Eur. Ceram. Soc. 35 (2015) 477–486.
[38] V. Krasnenko, M.G. Brik, First-principles calculations of the structural, elastic and electronic properties of MNxC1 − x (M = Ti, Zr, Hf; 0 ≤ x ≤ 1) carbonitrides at ambient and elevated hydrostatic pressure, Solid State Sci. 28 (2014) 1–8.
[39] S.-K. Sun, G.-J. Zhang, W.-W. Wu, J.-X. Liu, T. Suzuki, Y. Sakka, Reactive spark plasma sintering of ZrC and HfC ceramics with fine microstructures, Scripta Mater. 69 (2013) 139–142.
[40] L. Feng, S.-H. Lee, H.-L. Wang, H.-S. Lee, Nanostructured HfC–SiC composites prepared by high-energy ball-milling and reactive spark plasma sintering, J. Eur. Ceram. Soc. 36 (2016) 235–238.
[41] A.S. R, I.P. Borovinskaya, A.A. Gromov, E.A. Levashov, A.S. Mukasyan, Concise Encyclopedia of Self-Propagating High-Temperature Synthesis, (2017).